A&A 382, 1125–1137 (2002)
DOI: 10.1051/0004-6361:20011671

Astronomy & Astrophysics

Differential image motion at non-Kolmogorov distortions of the turbulent wave-front

P. F. Lazorenko[1,⋆]

Main Astronomical Observatory, National Academy of Sciencies of the Ukraine, Golosiiv, 252680 Kyiv-127, Ukraine

Received 25 May 2001 / Accepted 4 October 2001

Abstract. A description of image motion characteristics is given for a general case of atmospheric turbulence. For this purpose the parameter p used in the expression $F(q) \sim q^{-3-p}$ for a 2-D power spectrum of a phase is considered as a variable term with a typical 1/3–2/3 range of fluctuations. Dependence on p of the variance Δ^2 of differential image motion was studied for stellar configurations with one, two, and a set of reference stars located in a circular area, for a circular entrance pupil and interferometers. It was shown that for non-Kolmogorov turbulence, Δ^2 is subject to significant variations even when Fried's parameter r_0 and mean square absolute image motion are fixed. The method allowing us to reduce atmospheric errors by transition to 1-D measurements of differential coordinates is considered. Orientation of coordinate axes in this case depends on the direction of wind and intensity of turbulence in atmospheric layers. Atmospheric limitations of large ground-based telescopes are discussed.

Key words. atmospheric effects – instrumentation: interferometers – astrometry

1. Introduction

The distorting influence of the Earth's atmosphere on light wave propagation essentially restricts opportunities for ground-based telescopes and considerably reduces their efficiency in comparison with telescopes working in Space. In differential astrometry atmospheric factors affect apparent relative positions of closely located stars so that they are subject to random displacements.

Theoretical deductions of atmospheric influence on the process of star image formation are usually based on some model of atmospheric turbulence. Most frequently, the Kolmogorov type of the turbulence is used. With this approximation basic relations for fluctuations of a phase and amplitude of the light wave propagating in a turbulent medium have been obtained, and a theoretical description of various atmospheric effects in optical astronomy is given (e.g. Tatarsky 1961; Fried 1965; Martin 1987; Sarazin & Roddier 1990). Lindegren (1980), in particular, has found dependence of the mean error of differential measurements on parameters of turbulent layers, angles between stars, and exposure. Temporal spectra and asymptotic power laws for a phase difference and differential angle of arrival were studied by Conan et al. (1995).

Meteorological data (e.g. Vinnichenko et al. 1976; Bull 1967) and theoretical studies (Weinstock 1980; Dalaudier & Sidi 1987), however, testify that the real atmosphere is not always in that physical state of fully developed 3-D turbulence which is described by the Kolmogorov theory. Strong evidence of deviations from the Kolmogorov model of turbulent spectrum have been frequently detected by astronomical observations, for example, with optical interferometers (Bester et al. 1992; Buscher et al. 1995).

In the present paper, we study differential image motion suggesting a non-Kolmogorov type of the turbulence, and compare results with those known for a classical case. Description of differential displacements of star images is based on the model of a phase screen representing statistical properties of the wavefront. Spatial power spectral density of phase fluctuations is modeled by a power law with a spectral slope which depends on the type of turbulence in a layer. Tentative limits of the spectral index variations are estimated. A spectral approach to the problem allows one to take into account various cases of star relative positions and directions of image centroid measurements by introducing or modifying some necessary filters. Further, we derive expressions for the variance Δ of differential image motion, either averaged, or non-averaged with respect to the model spatial parameters, and discuss the

⋆ e-mail: gallaz@mao.kiev.ua

difference in performances of a filled single-aperture telescope and interferometer in very narrow fields.

2. A model of the phase screen

Direct and remote sensing of an atmosphere shows that intensive clear air turbulence exists only in a discrete set of narrow turbulent layers isolated from each other by laminar flows. A typical depth of turbulent layer Δh is much less than its height h above the surface, and is in the limit of 10–100 m (Barletti et al. 1977; Redfern 1991) to 100–800 m (Vinnichenko et al. 1976). According to Chunchuzov (1996), existence of the layered structure of turbulence is associated with features of a vertical profile of the Brunt–Vaisala frequency N. He also argues that near local maxima in the frequency N, vertical profile gravitational internal waves can create thin horizontal layers of a turbulence whose positions are independent of the type of internal wave source.

Small values of Δh allow one to use the model of a thin phase screen (Goodman 1985) for each turbulent layer. In the model, a layer thickness and extinction of light transmitting through a layer are neglected, only change of a phase is considered. A plane wave entering the screen gains some random phase $\phi(x, y)$ on exit, where x, y are rectangular coordinates of a point in the screen plane. Though orientation of the coordinate frame x, y is arbitrary, we assume for definiteness that its axes are parallel to the axes of the equatorial coordinate system. By statistical properties, $\phi(x, y)$ corresponds to a homogeneous and isotropic random field, so 2-D power spectral density $F_\phi(u, v)$ of a phase has circular symmetry: $F_\phi(u, v) = F_\phi(q)$. Here u, v are spatial frequencies corresponding to x, y, and $q = \sqrt{u^2 + v^2}$ is a circular frequency. For the function $F_\phi(q)$ with a fairly complicated dependence on q (Sect. 3) we use approximation by a simple function

$$\hat{F}_\phi(q) = c_\phi q^{-p-3},\ q_1 < q < q_2 \tag{1}$$

with fitting parameters p and c_ϕ. A good fitting of the function $F_\phi(q)$ by Eq. (1) is required only in the effective frequency range q_1, q_2 where most (for example, 90%) of the variance of differential image motion is generated. Such a definition of model parameters allows us without a loss in the accuracy of future simulations to use infinite integration limits over frequency q. The value of frequency q_1 depends on the vertical structure of the turbulent atmosphere, location of observed stars and direction of axes along which image centroids are measured. Scales q_1^{-1} are typically in the limits 100–1000 m (Sect. 5), but in a special 1-D mode of observations $q_1^{-1} \approx 10^5$ m (Sect. 6). The frequency q_2 is determined largely by the telescope aperture, so $q_2 \sim D^{-1}$.

The factor c_ϕ in (1) is determined by the intensity of turbulent motions and is proportional to the coefficient C_n^2 of the structure function of refractive index n fluctations

$$D_n(r) = C_n^2 r^p, \tag{2}$$

where r is a distance between two points in 3-D space. The use of C_n^2 in Eq. (2) is usually associated with a fully developed Kolmogorov turbulence which is isotropic in 3-D space. In this classic case $p = 2/3$ and a relation

$$c_\phi = 0.033(2\pi/\lambda)^2(2\pi)^{-2/3}C_n^2\Delta h \tag{3}$$

is valid (Tatarsky 1961). For isotropic turbulence but arbitrary $p \neq 2/3$, expression (3) is substituted by a more general one. A relevant relation can be derived from the expression (Tatarsky 1961) that determines dependence of the phase structure function $D_\phi(r) = \langle[\phi(\boldsymbol{r'} + \boldsymbol{r}) - \phi(\boldsymbol{r'})]^2\rangle$ on the distance r between points $\boldsymbol{r'}$ and $\boldsymbol{r'} + \boldsymbol{r}$ in the plane of the phase screen (angle brackets denote ensemble average)

$$D_\phi(r) = (2\pi/\lambda)^2(C_n^2\Delta h)r^{p+1}W. \tag{4}$$

Here λ is a wavelength, $W = \int_{-\infty}^{\infty}[(u^2+1)^{p+2} - u^p]\,\mathrm{d}u$ and the use of the variable p instead of its numerical value 2/3 is introduced. On the other hand, the phase structure function is related to the power spectral density (1) by expression

$$D_\phi(r) = 2\int_0^\infty \int_0^{2\pi} [1 - J_0(2\pi qr)]\hat{F}_\phi(q)q\,\mathrm{d}q\,\mathrm{d}\varphi, \tag{5}$$

where J_0 is the Bessel function. Having integrated and compared the result with (4), we obtain

$$c_\phi = R(2\pi/\lambda)^2(2\pi)^{-p}C_n^2\Delta h, \tag{6}$$

where

$$R = \frac{2^p(p+1)^2}{4\pi^2}W\Gamma\left(\frac{1+p}{2}\right)/\Gamma\left(\frac{1-p}{2}\right). \tag{7}$$

At $p = 2/3$ and $R = 0.033$ Eq. (6) is transformed to (3).

Note that at greater scales isotropy is not maintained (Sect. 3) and Eqs. (4) and (6) are not valid.

In addition to the already introduced parameters, the model (1) is supplemented with data on module V and the angle ε that wind velocity vector $\boldsymbol{V}$ forms with the x-axis.

3. General characteristics of the temperature and phase turbulent spectra

The spatial spectrum of phase fluctuations, besides being directly related to that of temperature t fluctuations in a turbulent layer, depends also on localization of a turbulence which can be either 3-D or 2-D, concentrated in a narrow horizontal quasi-2-D space.

To begin, let's refer to results of meteorological studies of a turbulent temperature spectrum under clear sky conditions on scales $1-10^5$ m, of interest for this study.

By the data of airborne measurements in the troposphere and lower stratosphere (Vinnichenko et al. 1976), a 1-D temperature spectrum $F_t'(q)$ in a low-frequency spectral range usually follows a dependence $F_t'(q) \sim q^{-3}$ which in the higher frequency range is transformed to

$F'_t(q) \sim q^{-5/3}$. The position of the frequency q_B separating these spectral ranges is not permanent and depends on stratification. In diagrams presented by Vinnichenko et al. (1976), q_B corresponds to scales of 200–1000 m. Spectral slopes intermediate between $-5/3$ and -3 are also frequently found, and sometimes spectra of unregular shapes with local maxima and minima are detected.

Observed features of the function $F'_t(q)$ in general are consistent with modern theories of atmospheric turbulence. According to Dalaudier & Sidi (1987), in low frequencies (buoyancy range) temperature fluctuations are caused by vertical displacements of air particles in a stably stratified medium, some part of kinetic energy is converted here to the potential form. A spectral flux of potential energy (temperature) in the buoyancy subrange is directed towards larger scales. In this subrange both $F'_t(q)$ and the kinetic energy spectrum follow a dependency $\sim q^{-3}$. In higher frequencies (passive range of temperature fluctuations corresponding to an inertial range of kinetic energy) temperature fluctuations are converted to heat in the usual way described by the Kolmogorov theory. Here the spectral slope is $-5/3$. Dalaudier & Sidi (1987) theoretically have substantiated a possibility of the so-called "spectral gap" occurrence nearby q_B, with an adjacent peak at higher frequency. The slope of the spectral curve to the right of the gap is much less than $-5/3$. Weinstock (1980) suggested some other mechanisms leading to the formation of similar gaps in the kinetic energy spectrum on scales of 30–1000 m.

In Table 1, typical scales for buoyancy and passive subranges of turbulence, corresponding theoretical power laws for function $F'_t(q)$ and structure functions of t and n quantities are given. It should be noted that "theoretical" power laws are deduced under the classical assumption of no additional sources and sinks of energy (wind shear, gravitational waves), and therefore are rather approximate.

The slopes of observed spectral functions $F'_t(q)$ frequently and in a random way deviate from the "theoretical" ones. This was noticed, for example, by Bull (1967) who studied temporal spectra of n index measured with a microwave refractometer. While an average spectral slope was -1.68 at scales 2–100 m (temporal frequencies transformed into spatial scales with $V = 5$ m/s), which is very close to the Kolmogorov's $-5/3$, sampled values of the spectral index varied from -1.2 to -2.5. Additional, modifying influences on the theoretically predicted temperature spectrum were affected by internal gravitational waves (Hogstrom et al. 1998).

The indicated details of the function $F'_t(q)$ shape directly affect the phase power spectral density $F_\phi(q)$. Function $F_\phi(q)$, besides, depends on the type of spatial (2-D or 3-D) localization of the turbulent temperature field, that is, on the dimensionality of space where the temperature fluctuations can be considered as isotropic. On small scales not exceeding the thickness of a turbulent layer Δh or outer scale of turbulence L (these value estimates range from 3–5 m (Coulman et al. 1988), to 30–100 m (Busher et al. 1995) and to 100–1000 m (Vinnichenko et al. 1976), fluctuations are 3-D and basic functions of a phase are determined by expressions (1) and (4). Therefore, with a "theoretical" spectrum $F'_t(q) \sim q^{-5/3}$ we have here (first line in Table 1) $D_\phi(r) \sim r^{5/3}$, $F'_\phi(q) \sim q^{-11/3}$ and $p = 2/3$.

On scales $q^{-1} \gg \Delta h$ and $q^{-1} \gg L$ the turbulence is essentially 2-D. The power spectral densities and structure functions of n and t are described here (in a horizontal plane) by the same power laws as for 3-D turbulence. Corresponding functions for a phase, however, are modified. Really, on scales $r \gg \Delta h$ one can neglect changes of n and t across a layer. Accordingly, a phase difference $\phi(\boldsymbol{r}' + \boldsymbol{r}) - \phi(\boldsymbol{r}') = \frac{2\pi}{\lambda}[n(\boldsymbol{r}' + \boldsymbol{r}) - n(\boldsymbol{r}')]\Delta h$ between two points of the screen $(\boldsymbol{r}' + \boldsymbol{r})$ and $\boldsymbol{r}'$ is proportional to the difference $t(\boldsymbol{r}' + \boldsymbol{r}) - t(\boldsymbol{r}')$, hence the phase structure function $D_\phi(r)$ is proportional to the structure functions of n and t. So, in a passive range $D_\phi(r) \sim r^{2/3}$, while in the buoyancy range $D_\phi(r) \sim r^2$ is expected (Table 1). Now, using Eq. (5) it is easy to find spectral densities of a phase $F'_\phi(q) \sim q^{-4}$ (buoyancy range) and $F'_\phi(q) \sim q^{-8/3}$ (passive range) corresponding to these functions. Two values of parameter p for 2-D turbulence are therefore valid: $p = +1$ at very large scales $q^{-1} > q_B^{-1}$, and $p = -1/3$ for scales shorter than q_B^{-1}. Thus, the function $F_\phi(q)$ relevant even to a very simplified theoretical description of a turbulence, on scales $1-10^5$ m depends on frequency in a rather complicated way.

Discussion of astronomical sources of data of the parameter p, in view of astronomical applicability of this analysis, is of a special value.

Diagrams of phase structure functions, temporal spectra, and Allan functions are very typical for path differences from a star to two telescopes of infrared interferometer with baselines 4 and 13 m (Bester et al. 1992). The peculiarity of these diagrams over spatial scales $2 \times 10^1 - 10^4$ m (at wind velocity $V = 10$ m/s corresponding to temporal scales 2–1000 s and frequencies 10–0.5 Hz) is in a strongly varying form of observed functions from sample to sample. For scales indicated, the parameter p ranged from 0.2 to 1.0 with an average $p = 0.5$.

Similar results in the low-frequency spectral domain were obtained by Busher et al. (1995) with a MARK-III interferometer. Temporal spectra of phase differences at 0.001–0.1 Hz (scales $10^2 - 10^4$ m at $V = 10$ m/s) had distinct deviations from the Kolmogorov type of the spectrum, displayed mainly as the decrease of p. In 16% of cases the flat spectra relevant to $p = 0$ were obtained. In the high-frequency 3–40 Hz region (scales 0.25–3 m) the dispersion of individual values of p was smaller, 90% of which did not exceed the limits 0.4–0.7. On average $p = 0.55$.

Coulman & Vernin (1991) analysed observations of stars with NRAO's Very Large Array of radio telescopes (Armstrong & Sramek 1982) at baselines from 50 m up to 22 km.

Table 1. Theoretical structure functions and power spectra of the temperature t, refractive index n, and phase ϕ for different types and scales of a turbulence, and effective parameter p.

spatial scales	spectral subrange	spatial form of the turbulence	structure functions		power spectrum		p
			n and t	ϕ	n and t	ϕ	
from 1 m to $10-10^3$ m	passive	3-D	$r^{2/3}$	$r^{5/3}$	$q^{-5/3}$	$q^{-11/3}$	+2/3
from $10-10^2$ m to 10^2-10^4 m	passive	2-D	$r^{2/3}$	$r^{2/3}$	$q^{-5/3}$	$q^{-8/3}$	−1/3
from 10^2-10^3 m to 10^5 m and more	buoyancy	2-D	r^2	r^2	q^{-3}	q^{-4}	+1

At moderate baselines 100–1200 m they found that $D_\phi(r) \sim r^{0.43}$ represents both autumn and winter observations, and $D_\phi(r) \sim r^{1.11}$ does so for a spring and summer period. On scales considered, the turbulence is intermediate between 2-D and 3-D, thus logarithmic slopes of the phase structure functions in the 2/3–5/3 range are expected (Table 1). Observed slopes, however, are consistent with the expected range only for the spring to summer observations. Corresponding mean values of p are −0.57 and +0.11 for the two periods.

It should be noted that the well-known Hog's (1968) model of the frequency spectra of absolute image motion based on observational data of various types has a parameter corresponding to $p = 0.5$.

Lazorenko (1992), analyzing photographic and visual data on star image tracks obtained for site testing programmes, has shown that the shape of autocorrelation functions and power spectra of image motion is usually highly biased in consequence of a limited duration of observational series. The absolute image motion spectrum corrected for this effect should have a maximum at 0.01–0.015 Hz (scales 600–1000 m at $V = 10$ m/s). It was found that $p = 0.97$ at higher frequencies, and at lower frequencies $p < 0$, which agrees well with the data in Table 1.

This short review of meteorological, astronomical, and theoretical data allows us to make following conclusions:

1) the samplings of p have an intrinsic scatter caused by changes of physical conditions in the atmosphere,

2) on scales 1–300 m giving a main contribution to the variance of differential image motion, p varies at least from 1/3 up to 2/3, with a mean value of about 0.5,

3) on scales 200–1000 m the function $F_\phi(q)$ has a smaller slope, with p decreasing sometimes to negative magnitudes.

4. Spatial power spectral density

The magnitude of differential displacement is a function of the phase screen parameters c_ϕ, p, h, V and ε, and depends on location of the program object with respect to a reference frame. The direction along which the differences of coordinates of star image centroids are measured is also of importance. Taking into consideration a vast variety of possible configurations of reference stars, we shall examine only those which are most typical.

a) Two stars, located in the sky at angular distance ρ. At some points A and B a phase screen is crossed by light beams passing from these stars to the centre of the telescope pupil. Here and further, point A refers to the target star while point B refers to the geometrical centre of the reference frame (in this instance, to star B). The line AB is the baseline of configuration.

b) Two reference stars B_1 and B_2, seen at an angle ρ. The program star A is on a common arc with reference stars shifted some angle ρ' off their middle point B. B_1B_2 is the baseline of configuration.

c) A set of some reference stars, located uniformly in a circular area. In the limit stars completely fill in the area forming a circle of angular diameter ρ with the target star A displaced some angle ρ' off the circle centre B.

Each configuration projected to the phase screen is characterized by its linear size $S = h\rho$, the distance between the geometrical centres of star systems $S' = h\rho'$ (for the elementary configuration "a" $S = S'$ and $\rho = \rho'$ is assumed), and angle ψ the baseline formed with the x-axis.

With light rays propagating perpendicularly to a wave-front, the star image displacements in the focal plane are proportional to the mean gradient of the phase taken over the screen section involved in image formation at exposure T. It should be noted that axes of the coordinate system ξ, η, in reference to which positions and displacements of stars are measured, may not necessarily be parallel to the x, y axes fixed by the celestial frame. The angle between the axes of these coordinate frames is here denoted θ. Differential displacement $\Delta\xi$ in the direction of the ξ-axis is equal to the difference of displacements of the target star and a system of reference stars. An efficient approach for studying statistical properties of various parameters relevant to the turbulent wave-front phase, and based on the use of convolution operators, was described by Conan et al. (1995). Using his formalism, it is easy to derive the following expression which we give in polar coordinates r, φ':

$$\Delta\xi(\boldsymbol{r}) = \frac{\lambda}{2\pi}\frac{\partial\phi(\boldsymbol{r})}{\partial r_\xi} * \mathrm{rect}\left[\frac{r\cos(\varphi'-\varepsilon)}{VT}\right] * P(\boldsymbol{r}/D) * \tilde{Q}(\boldsymbol{r}) \cdot (8)$$

Here $\Delta\xi$ is considered as a 2-D function of the vector $\boldsymbol{r}$ specifying the position of the point B on the phase screen. Eq. (8) describing a linear filtration of the phase $\phi(\boldsymbol{r})$ is a

sequential convolution of four functions corresponding to following the procedures:

- calculation of the phase gradient $\partial/\partial r_\xi$ in the direction of the ξ-axis rotated by θ from the x-axis;

- calculation of the running average over a straight 1-D line VT oriented along the wind

$$\mathrm{rect}[z/(VT)] = \begin{cases} (VT)^{-1}, & |z| \le VT/2 \\ 0, & |z| > VT/2; \end{cases} \quad (9)$$

- averaging over the telescope aperture D

$$P(\boldsymbol{r}/D) = \begin{cases} 4/(\pi D^2), & r \le D/2 \\ 0, & r > D/2; \end{cases} \quad (10)$$

- evaluation of a difference between two values of a function in points A and B, which for configurations "a", "b", and "c" is correspondingly:

$$\tilde{Q}(\boldsymbol{r}) = \begin{cases} \delta(\boldsymbol{r}+\boldsymbol{S}) - \delta(\boldsymbol{r}) \\ \delta(\boldsymbol{r}+\boldsymbol{S}') - [\delta(\boldsymbol{r}+\boldsymbol{S}/2) + \delta(\boldsymbol{r}-\boldsymbol{S}/2)]/2 \\ \delta(\boldsymbol{r}+\boldsymbol{S}') - P(\boldsymbol{r}/S)\cdot \end{cases} \quad (11)$$

Here $\boldsymbol{S}$ is a vector relevant to the baseline S, and $\boldsymbol{S}'$ is that for offset S' of the star systems.

Expressions of the type (11) may be easily modified for other stellar configurations. Note that Eq. (11) for configuration "b" is valid even if the star A is not in line with reference stars.

The use of convolution operators in Eq. (8) allows direct proceeding to the analysis in the spectral domain. In this case the spatial power spectral density of $\Delta\xi$ in polar coordinates q, φ is expressed as a sequential product of $\hat{F}_\phi(q,\varphi)$ and four filters originating from the corresponding functions in Eq. (8) and their Fourier transforms:

$$\begin{aligned} F(q,\varphi) = {} & \hat{F}_\phi(q,\varphi)[\lambda q\cos(\varphi-\theta)]^2 \\ & \times \mathrm{sinc}^2[\pi VTq\cos(\varphi-\varepsilon)] \\ & \times \mathrm{somb}^2(\pi Dq) Q^2(q,\varphi)\cdot \end{aligned} \quad (12)$$

Here $\mathrm{sinc}(z) = \sin(z)/z$, and $\mathrm{somb}(z) = 2J_1(z)/z$. Filter $Q^2(q,\varphi)$ is defined by the geometrical positions of stars, that is by the function $\tilde{Q}(\boldsymbol{r})$. If the latter is given by Eq. (11), then

$$Q^2(q,\varphi) = \begin{cases} 2\{1-\cos[2\pi qS\cos(\varphi-\psi)]\} & \text{"}a\text{"}, \\ 1+\cos^2[\pi qS\cos(\varphi-\psi)] & \\ -2\cos[\pi qS\cos(\varphi-\psi)] & \\ \times\cos[2\pi qS'\cos(\varphi-\psi)] & \text{"}b\text{"}, \\ 1-2\cos[2\pi qS'\cos(\varphi-\psi)] & \\ \times\mathrm{somb}(\pi qS)+\mathrm{somb}^2(\pi qS) & \text{"}c\text{"}. \end{cases} \quad (13)$$

For configuration "b" with the star A being off the line B_1B_2:

$$\begin{aligned} Q^2(q,\varphi) = {} & 1+\cos^2[\pi qS\cos(\varphi-\psi)] \\ & -2\cos[\pi qS\cos(\varphi-\psi)]\cos(2\pi\boldsymbol{q}\boldsymbol{S}')\cdot \end{aligned} \quad (14)$$

It is useful to write functions $Q^2(q,\varphi)$ averaged with respect to the angle ψ of baseline orientation, and $S'=0$:

$$Q^2(q) = \begin{cases} 2[1-J_0(2\pi qS)] & \text{"}a\text{"} \\ 2\{1-J_0(\pi qS)-\frac{1}{4}[1-J_0(2\pi\boldsymbol{q}\boldsymbol{S})]\} & \text{"}b\text{"} \\ [1-J_0(\pi qS)-J_2(\pi qS)]^2 & \text{"}c\text{"}. \end{cases} \quad (15)$$

The variance of differential displacement Δ^2 is

$$\Delta^2(\theta,\varepsilon,\psi) = \int_0^{2\pi}\int_0^\infty F(q,\varphi) q\,\mathrm{d}q\,\mathrm{d}\varphi \quad (16)$$

In particular, for configuration "a"

$$\begin{aligned} \Delta^2 = {} & 2\lambda^2 c_\phi \int_0^{2\pi}\int_0^\infty q^{-p}\cos^2(\varphi-\theta) \\ & \mathrm{sinc}^2[\pi VTq\cos(\varphi-\varepsilon)] \\ & \times\{1-\cos[2\pi qS\cos(\varphi-\psi)]\}\mathrm{somb}^2(\pi Dq)\,\mathrm{d}q\,\mathrm{d}\varphi. \end{aligned} \quad (17)$$

5. The variance of differential image motion averaged with respect to the wind and baseline orientations

Although the power spectrum $F(q,\varphi)$ (12) and the variance Δ^2 (16) are functions of three spatial angles ψ, ε and θ, only two of them are independent due to the arbitrary choice of φ angle origin. Therefore integration, or averaging $\Delta^2(\psi,\varepsilon,\theta)$ over a couple of angular parameters in the limits $0-2\pi$ results in a new variance Δ_0^2 which is completely independent of the relative orientation of stars, coordinate axes, and direction of the wind. Setting conditions on angular differences like $\theta-\psi=0$, $\varepsilon-\theta=0$ etc. leads to similar results.

The effect of averaging over ε is created in a natural way by fluctuations and changes with height of the wind direction. Though there are a few possible ways and sources of performing averaging of the variance (16) over angular parameters, further consideration shows that in some instances the resulting quantities follow a similar dependency on T and angular size ρ, the details of reference star distribution in the field being of less importance. This Section deals with the variance Δ which, owing to averaging, does not depend on angular parameters.

Let's consider a case of some randomly distributed pairs of stars (configuration "a") with equal baseline length $S = h\rho$. The direction along which the angular distance between stars of the pair is measured usually either coincides with the direction of the baseline ($\theta-\psi = 0, \pm\pi$), is perpendicular to that of ($\theta-\psi = \pm\pi/2$), or directed along the x-axis ($\theta=0$) or y-axis ($\theta=\pi/2$). We shall denote the relevant quantities of Δ as $\Delta_\parallel$, $\Delta_\perp$, Δ_x, and Δ_y, and introduce their average

$$\bar{\Delta}^2 = \frac{\Delta_x^2+\Delta_y^2}{2} = \frac{\Delta_\parallel^2+\Delta_\perp^2}{2} = \frac{1}{2\pi}\int_0^{2\pi}\Delta^2(\theta,\varepsilon,\psi)\,\mathrm{d}\theta. \quad (18)$$

Owing to the factor $\cos^2(\varphi-\theta)$ in Eq. (17), the variance $\bar{\Delta}^2$ is equal to Δ^2 continuously averaged over θ in the limits $0-2\pi$. Δ_0^2 is found by further averaging of the variance (18) over ψ:

$$\begin{aligned} \Delta_0^2 = {} & \frac{1}{4\pi^2}\int_0^{2\pi}\int_0^{2\pi}\Delta^2(\theta,\varepsilon,\psi)\,\mathrm{d}\theta\mathrm{d}\psi \\ = {} & 4\lambda^2 c_\phi\int_0^\infty q^{-p} I(\pi VTq)[1-J_0(2\pi qS)] \\ & \times\mathrm{somb}^2(\pi Dq)\,\mathrm{d}q \end{aligned} \quad (19)$$

where

$$I(z) = \int_0^{\pi/2} \frac{\sin^2(z\cos\beta)}{z^2\cos^2\beta}\,\mathrm{d}\beta = \frac{\pi}{z}\sum_{n=1}^{\infty} J_{2n-1}(2z) - \frac{\pi}{2z}J_1(2z)\cdot \quad (20)$$

To obtain this expression, one may expand the function $\mathrm{sinc}^2(x) = [1-\cos(2x)]/2x^2$, where $x = z\cos\beta$ in the power series of the argument, and integrate it over β in the limits $0-\pi/2$. Then, using the identity $\sum_{n=1}^{\infty} J_{2n-1}(2z) = \int_0^{2z} J_0(2t)\,\mathrm{d}t$, with the function $J_0(2t)$ expanded into a power series of t, integration yields result equal to the expression given above. The function $I(z)$ (Fig. 1) allows the simple approximation

$$I(z) = \begin{cases} \pi/2, & z \le 1 \\ \pi/(2z), & z > 1 \end{cases} \quad (21)$$

and for large z decreases as z^{-1}, much slower than the original function $\mathrm{sinc}^2(z) \sim z^{-2}$. A $(VT)^{-1}$ dependence of Δ^2 on T for large exposures $VT \gg S$ thus directly follows from approximation (21). Another behaviour $\Delta^2 \sim (VT)^{-2}$ is also possible if no averaging of the function $\mathrm{sinc}^2[\pi VTq\cos(\varphi-\varepsilon)]$ is performed (Sect. 6).

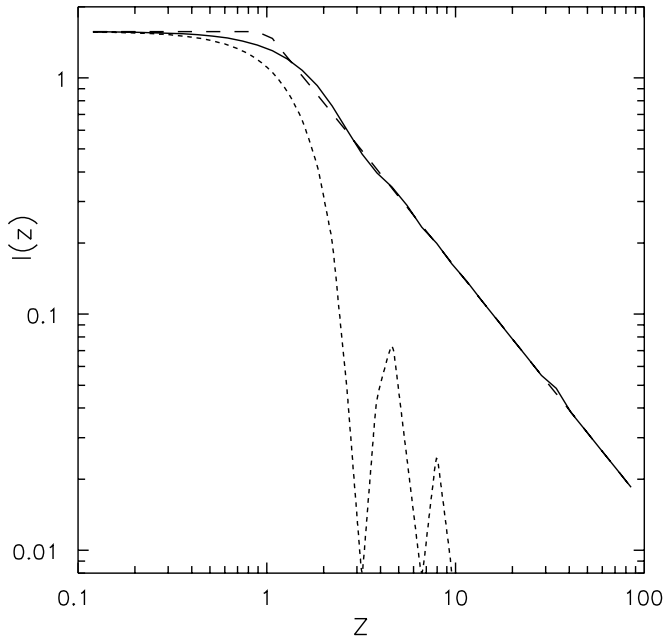

Fig. 1. The function $I(z)$ (solid), its approximation by Eq. (21) (long dashed), and the function $\mathrm{sinc}^2(z)$ (short dashed).

5.1. Wide angular separations

Figure 2 shows the function $\Delta_0\sqrt{T}$ and its dependence on ρ calculated using Eq. (19) with $p = 2/3$, $T = 100$ s, and $D = 0.78$ m (aperture of the MAP, Gatewood 1987). The atmosphere was represented by a single-layer model with parameters

$$h/V = 200 \text{ s},\ V = 14 \text{ m/s},\ \sigma_{30} = 0.14''. \quad (22)$$

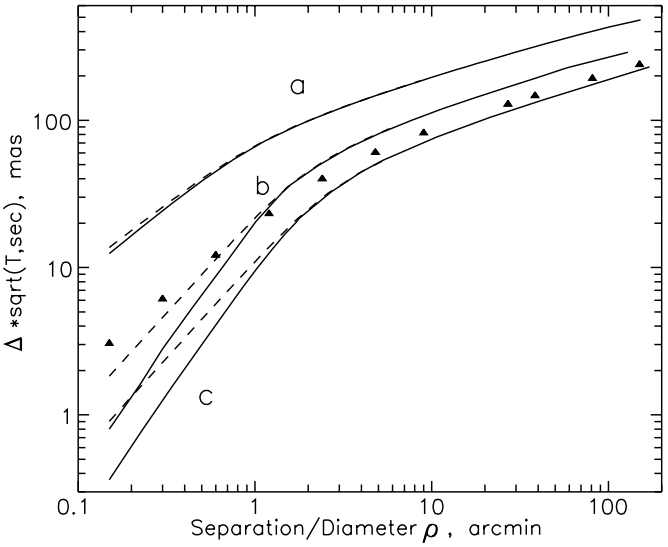

Fig. 2. Dependence of the variance $\Delta_0 T^{-1/2}$ on geometrical size ρ of stellar configurations described in Sect. 4: **a)** (binary star), **b)** triple star, and **c)** (circular distribution of reference stars). Solid lines – filled circular aperture $D = 0.78$ m; dashed lines – interferometer of equal baseline d. The case of a target star displaced $\rho' = 0.25\rho$ off the center of reference frame (configuration **c)**) is shown by triangles.

As a measure of a turbulence, we introduce here the mean value of absolute image motion σ_{T} (23) for small-aperture telescopes at exposure $T = T_{30} = 30$ s.

The values of h/V and V in (22) are approximately equal to the weight-average parameters used by Lindegren (1980) for differential effect evaluation at normal conditions of multi-layered atmosphere. In this sense parameters (22) represent "typical" atmospheric conditions, though they are used in this paper exceptionally for the purpose of qualitative interpretation of the expressions obtained. A normalizing coefficient c_ϕ is introduced in (22) implicitly, through σ_{30}. Such an approach to the calibration of Δ^2 in our opinion has some advantages. So, the quantity σ_{T} unlike c_ϕ has a clear astronomical sense and a rich history of determinations. Besides, σ_{30} is equal to the accuracy of meridian observations at $T_{30} = 30$ s, and is known to be in the limits $0.12-0.14''$, which follows also from the model of absolute motion power spectrum derived by Hog (1968). The use of σ_{30} instead of c_ϕ for calibration of the expression (19) is also more convenient, as in some cases it reduces the number of model parameters. For example, while two parameters h and V are used in Eq. (24), (25) contains only their ratio h/V which can be considered as a single parameter.

The expression relating σ_{T} and c_ϕ is found from (19) in the limit $S \to \infty$, $D \to 0$:

$$\sigma_{\mathrm{T}}^2 = \frac{\pi^p \lambda^2 c_\phi}{p(1-p)}\Gamma\left(\frac{3-p}{2}\right)/\Gamma\left(\frac{3+p}{2}\right)(VT)^{p-1}. \quad (23)$$

With parameter (22), $T = T_{30}$ and $p = 2/3$ we find $\lambda^2 c_\phi = 0.0154('')^2\ \mathrm{m}^{1/3}$. In spite of being calculated at $T = 100$ s, the function $\Delta_0\sqrt{T}$ in Fig. 2 represents well

any long exposures $T \gg h\rho/V$ and $T \gg D/V$. This circumstance, already noted by Lindegren (1980) and Han (1989), follows also from Eqs. (19) and (21). The function has two asymptotes: $\Delta_0\sqrt{T} \sim \rho^{p/2}$ at $h\rho \gg D$, and $\Delta_0\sqrt{T} \sim \rho$ at $h\rho \ll D$. In the first case direct integration of expression (19) with approximation (21) yields expansion of the variance in powers of ρ which, including the ρ^2 term, is

$$\Delta_0^2 = 2\lambda^2 c_\phi \pi^p [\Gamma(1-p/2)/\Gamma(1+p/2)](VT)^{-1} \times \left\{ \frac{(h\rho)^p}{p} - \frac{(h\rho)^2}{(3-p)(2-p)(VT)^{2-p}} \right\}, D \ll h\rho. \quad (24)$$

With normalization based on σ_{30}

$$\Delta_0^2 = \sigma_{30}^2 \frac{8\Gamma(1-p/2)\Gamma(3/2+p/2)}{p\Gamma(p/2)\Gamma(1/2-p/2)} \left(\frac{h\rho}{VT_{30}}\right)^p \left(\frac{T_{30}}{T}\right). \quad (25)$$

In the case of variances $\Delta_\parallel^2$ and $\Delta_\perp^2$ evaluated with additional averaging over the angle ψ, one may notice that integration of Eq. (17) over φ in both cases leads to a 1-D integral of the type (19), in which the factor $1 - J_0$ is replaced either on $1 - J_0 + J_2$ (for $\Delta_\parallel^2$), or on $1 - J_0 - J_2$ (for $\Delta_\perp^2$). At condition $D \ll S \ll VT$ further calculations with the use of approximation (21) yield

$$\Delta_\parallel^2 = \frac{2(p+1)}{p+2}\Delta_0^2,\ \Delta_\perp^2 = \frac{2}{p+2}\Delta_0^2. \quad (26)$$

The inequality $\Delta_\perp^2 < \Delta_0^2 < \Delta_\parallel^2$ shows that filtration of phase distortions for measurements directed perpendicular to a baseline is most efficient. Using Eqs. (24) and (26), one may derive an expression for $\Delta_\parallel^2$ which is very close to that obtained by Lindegren (1980) by means of an analysis performed in terms of phase structure functions. The ratio of these variances

$$\Delta_{\rm Lind}^2/\Delta_\parallel^2 = \frac{\sqrt{\pi}\Gamma[(p+4)/2]}{2\Gamma[(p+3)/2]} \quad (27)$$

is 1.12 at $p = 2/3$. The discrepancy of results is quite small and caused by different procedures of averaging over ψ. Thus, the variances Δ_0^2 and $\Delta_\parallel^2$, defined here by Eqs. (24), (26) correspond to the integral (continuous) averaging over ψ, while Lindegren assumed $\Delta_{\rm Lind}^2 = 0.5\Delta_{\rm max}^2$ where $\Delta_{\rm max}^2$ is the variance (17) calculated at $\psi - \varepsilon = \theta - \varepsilon = 90^0$.

For a single-layer model of an atmosphere with parameters (22), $p = 2/3$, and $\rho = 10'$, the use of Eqs. (25) and (26) allows one to find $\Delta\sqrt{T} = 0.233''$, where T is expressed in seconds. At arbitrary atmospheric parameters and $D \ll S \ll VT$

$$\Delta_\parallel = 0.233'' \left(\frac{\sigma_{30}}{0.14''}\right) (\rho/10')^{1/3} [(h/V)/200\ {\rm s}]^{1/3} T^{-1/2}, \quad (28)$$

where ρ is expressed in arcminutes, h/V and T in seconds. A very close estimate $\Delta_{\rm Lind}\sqrt{T} = 0.21''$ was derived by Lindegren (1980) who used a different approach to normalization based on intensity of the turbulence.

A similar power law of Δ^2 dependence on geometric size ρ of a stellar group is seen for configurations "b" and "c" (Fig. 2). Calculations were carried out using Eqs. (12) and (16) with the same parameters at which the curve "a" was plotted, with a central position of the target star ($\rho' = 0$), and with averaging over two (one in the case "c") angles, the function $Q^2(q)$ taken from (15). Both curves at wide ρ follow a power law $\rho^{p/2}$, are parallel to, and below the curve "a". The most efficient, of course, is filtration of phase distortions for configuration "c". Equation (16) under the condition $\rho h \ll VT$ in this case transformes to

$$\Delta_{\rm c}^2 = \frac{\lambda^2 c_\phi}{VT} \int_0^\infty q^{-p-1} [1 - J_0(\pi q S) - J_2(\pi q S)]^2 \times {\rm somb}^2(\pi D q)\, {\rm d}q \quad (29)$$

which for $\rho h \gg D$ simplifies to

$$\Delta_{\rm c}^2 = \frac{\pi^p \lambda^2 c_\phi}{VT} S^p E(p) = \frac{p\Gamma(1+p/2)}{2\Gamma(1-p/2)} E(p)\Delta_0^2. \quad (30)$$

Here the quantity

$$E(\gamma) = \int_0^\infty q^{-\gamma-1}[1 - J_0(q) - J_2(q)]^2\, {\rm d}q = \frac{2^{-\gamma+2}\Gamma(1-\gamma/2)}{\gamma(\gamma+2)\Gamma(1+\gamma/2)} \left[1 - \frac{2^{\gamma+1}\Gamma(\gamma/2+3/2)}{\sqrt{\pi}\Gamma(3+\gamma/2)}\right], \quad (31)$$

is found from integration by parts and is valid for $0 < \gamma < 4$. The numerical expression at Δ_0^2 in Eq. (30) varies from 0.24 at $p = 0.5$ to 0.11 at $p = 1$.

Thus, a symmetric circular distribution of reference stars, in comparison to one reference star, ensures a decrease in the variance equivalent to a 5–9 times longer exposure. If $p = 2/3$, then $E(2/3) = 0.8458$, and

$$\Delta_{\rm c} = 0.431\Delta_0 = 0.090'' \left(\frac{\sigma_{30}}{0.14''}\right) (\rho/10')^{1/3} [(h/V)/200\ {\rm s}]^{1/3} T^{-1/2}. \quad (32)$$

The numerical factor in (32) is close to $0.097''$ found by Lindegren for normal atmospheric conditions.

The use of configuration "b" with two reference stars is also efficient. To find the relevant variance, it is useful to take advantage of the similarity of the function $Q^2(q)$ for configurations "a" and "b". The comparison of relevant expressions in Eq. (15) allows us to write

$$\Delta_{\rm b}^2 = \Delta_0^2(\rho/2) - \frac{1}{4}\Delta_0^2(\rho) = (2^{-p} - 1/4)\Delta_0^2 \quad (33)$$

where $\Delta_0^2(\rho/2)$ is the differential motion (24) of two stars with angular separation $\rho/2$. Numerical term at Δ_0^2 is in the limit 0.46–0.25 for $0.5 < p < 1$. In the case of $p = 2/3$ Eq. (33) can be written in the form of (32) with a numerical factor $0.12''$.

The value of Δ^2 is larger when the position of a target star is displaced off the geometrical centre B of reference frame. Estimation of this effect requires a term with non-zero S' of $Q^2(q)$ function (13) to be included into expression (29). The expression obtained for $S' < S$ and $\rho h \gg D$ is easily transformed to

$$\Delta_{\rm c}^2(S') = \Delta_{\rm c}^2 + 2^{2-p}\frac{S'^2}{S}\frac{\Gamma(1-p/2)}{\Gamma(1+p/2)}\Delta_{\rm c}^2 \quad (34)$$

where Δ_c^2 corresponds to the symmetric distribution. Thus, offset of the star A on $\rho' = 0.25\rho$ leads to about a 10% increase of Δ at large $h\rho \gg D$ (Fig. 2).

5.2. Very narrow fields

Inequality $h\rho \ll D$ defines which ρ are refered to as "very narrow". Depending on the effective h of a turbulent atmosphere which is typically 1–15 km, we estimate $0.2{-}3'$ as a threshold for a narrow field approximation with 1 m telescopes, and larger $20{-}300'$ angles for the 100 m aperture. Owing to effective averaging of the phase over entrance pupil, in the $h\rho \ll D$ domain slopes of all curves in Fig. 2 are essentially steeper. The curves "b" and "c" follow here a $\rho^{1.83}$ power law, while for the curves "a" and "c"(with $\rho' > 0$) the power law $\rho^{1.00}$ is more moderate. A difference in the function behaviour is caused by the position of the target star A being either exactly at the center B of the reference frame or shifted. The difference in geometry affects properties of the function $Q^2(q)$ in the frequency range $D^{-1} < q < (h\rho)^{-1}$. Thus, for asymmetric configurations "a" and "c" with $\rho' > 0$ the function $Q^2(q)$ follows $\sim q^2$ law, whereas its behaviour $\sim q^4$ is much smaller for symmetric distributions.

Differential motion for small ρ has already been studied by Lindegren (1980) who found

$$\Delta_1^2 = [a_1 S^2 D^{-2+p} - a_2 S^{2+p} D^{-2}](VT)^{-1},\ \text{"a"} \tag{35}$$

$$\Delta_2^2 = a_3 S^{2+p} D^{-2} (VT)^{-1},\ \text{"c"} \tag{36}$$

where a_1, a_2, a_3 are some model constants, incorporating also dependence on $C_n^2(h)$ and p. These results, however, do not completely conform to our graphical representation in Fig. 2. Thus, the calculated slope of the curve "c" is 1.83 while $(2+p)/2 = 1.33$ is expected from Eq. (36). The reason for such a discrepancy is that Eqs. (35, 36) were derived by Lindegren based on approximation of the telescope's entrance pupil by two points separated by a distance D. The model is directly relevant to optical interferometers, but seems to represent well also image motion for the filled circular pupil, at least its first-order behaviour. Effects of the second order, however, may be quite different for interferometers and one-aperture telescopes.

We now derive analytical expressions for the filled aperture. An approximate expression for Δ_0^2 (configuration "a") in small ρ domain is found from Eq. (19). Assuming $1 - J_0(2\pi qS) = (\pi qS)^2$ for $q < (\pi S)^{-1}$, and $1 - J_0(2\pi qS) = 1$ for $q > (\pi S)^{-1}$, we find an expression of the type (35)

$$\Delta_0^2 = \frac{8\pi^{p-1}\lambda^2 c_\phi}{2+p}\Big[\frac{\sqrt{\pi}\,\Gamma(1/2+p/2)\Gamma(1-p/2)S^2}{[\Gamma(1+p/2)]^2 D^{2-p}} - \frac{2(2+p)S^{3+p}}{(1+p)(3+p)D^3}\Big](VT)^{-1} \tag{37}$$

with another power law of the second term.

Concerning configurations "b" and "c", the use of Eq. (29) with approximation $\mathrm{somb}(z) = 2\sqrt{2/\pi}z^{-3/2}\sin z$ at $z > 1$, or $\mathrm{somb}^2(z) \sim 4/(\pi z^3)$ results in

$$\Delta_c^2 = 4\pi^{p-1}\lambda^2 c_\phi D^{-3} S^{p+3} E(3+p)(VT)^{-1},\ \rho h \ll D \tag{38}$$

$$\Delta_b^2 = \frac{(1-2^{-p-1})\Gamma(-3/2-p/2)}{4E(3+p)\Gamma(5/2+p/2)}\Delta_c^2,\ \rho h \ll D. \tag{39}$$

For "normal" atmospheric conditions (22) and $p = 2/3$, when $\lambda^2 c_\phi = 0.0154('')^2\ \mathrm{m}^{1/3}$, with $E(3\frac{2}{3}) = 0.06608$ we derive

$$\Delta_b = 22.6\ \mathrm{mas}\,\rho^{11/6} D^{-3/2} T^{-1/2} \tag{40}$$

$$\Delta_c = 9.68\ \mathrm{mas}\,\rho^{11/6} D^{-3/2} T^{-1/2} \tag{41}$$

where ρ is expressed in arcminutes, and D in meters.

The power law in Eqs. (38)–(41) differs from that in expression (36) again by a factor S/D. Such a difference is consistent with that in the second term of Eqs. (35) and (37). This may be explained using Lindegren's (1980) results. Considering an arbitrary distribution of n stars, he derived

$$\Delta^2 = n^{-2}\sum_i^n\sum_j^n\left[f(\rho_{0i}) - \frac{1}{2}f(\rho_{ij})\right], \tag{42}$$

where f stands for Δ_1^2, ρ_{ij} refers to the distance between stars i and j, and subscript 0 is used for the target star. Specifying Eq. (42), Lindegren assumed that differential motion of stars i and j depends only on their separation but not on spatial angles $\varepsilon, \theta, \psi$. Quite clearly, however, this assumption is valid only if a preliminary averaging with respect to spatial angles ε and θ has been performed (ψ is fixed for any given i, j). For that reason all variances in (42) are to be treated as Δ_0^2 in the sense of (19), so Eq. (42) is to be written as

$$\Delta^2 = n^{-2}\sum_i^n\sum_j^n\left[\Delta_0^2(\rho_{0i}) - \frac{1}{2}\Delta_0^2(\rho_{ij})\right] \tag{43}$$

where Δ_0^2 is given by Eq. (37). The variance Δ_c^2 is so generated by the second term in expression (35) for Δ_1^2, the leading ρ^2 term vanishing while field averaging is performed for symmetric star distributions "b" and "c". The very remark concerns variances (38) and (39) which are proportional to the second term in Eq. (37). Thus, the difference of power laws noted for symmetric configurations is a consequence of different filtering properties of filled aperture and interferometers.

5.3. Stellar interferometry

Description of differential image motion for stellar optical interferometers is easily performed based upon the spectral approach. The interferometric data on double star separations are obtained from the difference in phase

fringe position of stars (Shao & Colavita 1992) which can be written as a convolution

$$\Delta\phi(\boldsymbol{r}) = \phi(\boldsymbol{r}) * [\delta(\boldsymbol{r}+\boldsymbol{d}) - \delta(\boldsymbol{r})] * \tilde{Q}(\boldsymbol{r}). \quad (44)$$

Here $\boldsymbol{d}$ is the interferometer baseline vector, and $\tilde{Q}(\boldsymbol{r})$ is one of the functions (11) for some particular stellar group. Note that the factor $[\delta(\boldsymbol{r}+\boldsymbol{d})-\delta(\boldsymbol{r})]$ is of the function $\tilde{Q}(\boldsymbol{r})$ form for binary star "a" configuration.

Using Eq. (44), and a filter (9) describing wind (time) averaging, a power spectral density of image motion is found

$$\begin{aligned} F(q,\varphi) =& 2\hat{F}_\phi(q,\varphi)\left(\frac{\lambda}{2\pi d}\right)^2 \mathrm{sinc}^2(\pi T\boldsymbol{qV}) \\ &\times(1-\cos 2\pi\boldsymbol{qd})Q^2(q,\varphi)\cdot \end{aligned} \quad (45)$$

Here a factor $\lambda^2/(2\pi d)^2$ relates a phase difference and angular separation of stars, and Q^2 is one of the functions (13). Let the relative orientation of $\boldsymbol{d}$ and $\boldsymbol{S}$ vectors be random. Then, for a wind direction changing with height, averaging over all angular parameters yields

$$\begin{aligned} \Delta^2_{\rm int} =& 4\lambda^2 c_\phi \int_0^\infty q^{-p} I(\pi VTq) \\ &\times[1-J_0(2\pi qS)]\frac{[1-J_0(2\pi qd)]}{\pi^2 d^2 q^2}\,\mathrm{d}q \end{aligned} \quad (46)$$

for a binary star. In comparison to Eq. (19), this expression contains a factor $\frac{1-J_0(2\pi dq)}{(\pi dq)^2}$ instead of $\left[\frac{2J_1(\pi Dq)}{(\pi Dq)}\right]^2$. At large z they are proportional to q^{-2} and q^{-3} respectively, which explains why filtering properties of a circular aperture are better at equal d and D.

Evaluation of Eq. (46) for large separations S with an accuracy to the leading term gives an expression that exactly coincides with Eq. (24). For very narrow angles $S \ll d$ an expression obtained

$$\Delta^2_{\rm int} = \frac{2\pi^p\lambda^2 c_\phi}{pVT}\left[\frac{\Gamma(1-p/2)}{\Gamma(1+p/2)} - \frac{2}{2+p}\left(\frac{S}{d}\right)^p\right]\frac{S^2}{d^{2-p}} \quad (47)$$

is of the form (35). A ratio of $\Delta^2_{\rm int}$ to Δ^2_0 for a filled aperture (37) at $D = d$

$$\Delta^2_{\rm int}/\Delta^2_0 = \frac{\sqrt{\pi}}{2p}\frac{\Gamma(2+p/2)}{\Gamma(1/2+p/2)} \quad (48)$$

does not depend on S and is 1.40 for Kolmogorov turbulence. The curve in Fig. 2 which correponds to $\Delta_{\rm int}$ is parallel and above that for Δ_0.

Similarly, replacing a term $1-J_0(2\pi qS)$ in Eq. (46) by a proper function $Q^2(q)$ allows us to obtain expressions for other stellar configurations at small $S \ll d$:

$$\Delta^2_{\rm b} = \frac{(1-2^{-p})\pi^p\lambda^2 c_\phi\Gamma(1-p/2)}{p(2+p)\Gamma(2+p/2)}S^{2+p}d^{-2}(VT)^{-1} \quad (49)$$

$$\Delta^2_{\rm c} = \pi^p\lambda^2 c_\phi E(1+p)S^{2+p}d^{-2}(VT)^{-1} \quad (50)$$

where $E(1\frac{2}{3}) = 0.1550$. The power law $S^{2+p}d^{-2}$ obtained here is characteristic for all symmetric stellar groups observed with interferometers (Fig. 2), the resulting atmospheric influence being much smaller than for a binary star (47) and other asymmetric distributions (42).

Table 2. Differential image motion Δ (in μas) for large (10 m) and very large (100 m) interferometer and filled pupil, $T = 100$ s, stellar group size $\rho = 1'$ and Kolmogorov model.

conf.-n	offset	interferometer, d		filled pupil, D	
type	ρ'	10 m	100 m	10 m	100 m
"a"	-	1820	390	1530	330
"b"	0	180	18	70	2.3
"c"	0	150	15	30	1.0
"b"	$15''$	490	100	380	83

Table 2 shows the relative performance of an interferometer and filled aperture of large $d = D = 10$ m and very large $d = D = 100$ m size, $\rho = 1'$, moderate $T = 100$ s, Kolmogorov turbulence, and atmospheric layer (22). Due to a strong dependence of Δ^2 on h, the data given are only illustrative. Anyhow it clearly shows the great advantage of symmetric frames like "b" and "c". To achieve $\Delta \sim 1$ μas level with a $D = 100$ m telescope, a target star, however, should be exactly at the center of the reference frame. Analysis of Eq. (13) for a slightly non-central position of the target star ($0 < S' < S$) allows us to find approximation

$$\Delta^2(\rho') = \Delta^2_{\rm sym} + \Delta^2_0(\rho = \rho') \quad (51)$$

$\Delta^2_{\rm sym}$ corresponds here to the symmetric case, and $\Delta^2_0(\rho = \rho')$ is the non-centering error equal to the variance (37) for a binary star with $(\rho = \rho')$. The effect of offset is illustrated by the last row in Table 2, showing strong degradation in precision even at small shift $\rho' = \rho/4$. The non-centering term that follows dependence $\Delta_0 \sim \rho'$ (Eqs. (38) and (47)) may be reduced to the $\Delta_{\rm sym}$ level only at unexceptably small ρ'. Thus, with $D = 10$ m and 100 m apertures we estimate $\rho' < 1.2''$ and even $\rho' < 0.2''$.

5.4. Symmetrization of observed stellar groups

Any unregular and non-centered at the target star group of $n \geq 3$ stars, however, can be easily "symmetrized" with respect to the form of its Fourier transform $Q^2(q)$ by configuring it to the shape specific to geometrically perfect configurations "b" and "c". The procedure is aimed at eliminating q^2 terms in Q^2 expansion at low $q \ll S^{-1}$. The relative position of the target 0-star

$$\Delta\alpha = n^{-1}\sum_{i=1}^n a_i(\alpha_0 - \alpha_i); \Delta\delta = n^{-1}\sum_{i=1}^n a_i(\delta_0 - \delta_i) \quad (52)$$

is formed with weights a_i which meet equations

$$\sum a_i(\xi_i - \xi_0) = 0; \sum a_i(\eta_i - \eta_0) = 0; \sum a_i = n \quad (53)$$

where ξ_i, η_i are coordinates of i-star in the phase screen (or sky), and thus puts the weighted center of the group directly at the target. The function (11) corresponding to (52) is $\tilde{Q}(\boldsymbol{r}) = n^{-1}\sum a_i[\delta(\boldsymbol{r}) - \delta(\boldsymbol{r} - \boldsymbol{S}_i)]$ whence we find $Q^2(q)$ averaged over θ and ε as

$$\begin{aligned} Q^2(q) =& 1 - 2n^{-1}\textstyle\sum_i a_i J_0(2\pi q\rho_{0,i}h) \\ &+n^{-2}\textstyle\sum_{i,j} a_i a_j J_0(2\pi q\rho_{i,j}h) \end{aligned} \quad (54)$$

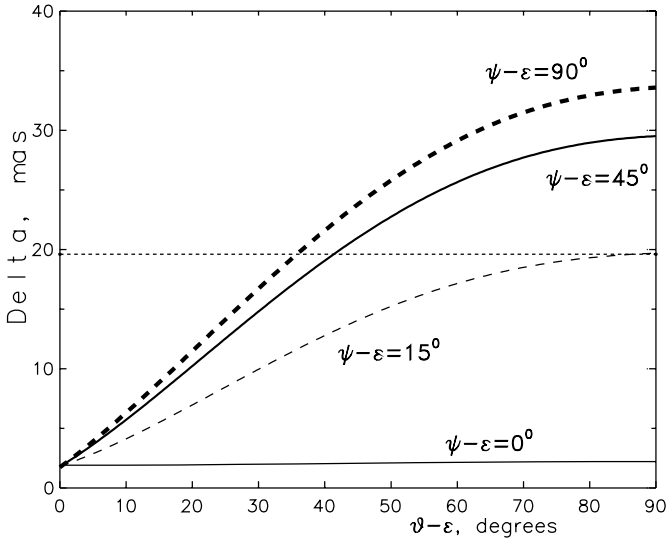

Fig. 3. Differential image motion Δ of two stars spaced $10'$ as a function of $\theta-\varepsilon$ at some fixed $\psi-\varepsilon$. Horizontal dashed line is the mean variance Δ_0, Eq. (19). Atmospheric parameters are the same as in Fig. 2, $p=2/3$, and $T=100$ s.

where $\rho_{i,j}$ is the distance between stars. Expanding $Q^2(q)$ into a power series of q, we notice that under conditions (53) all q^2 terms are cancelled out. Introduction of weights a_i thus modifies any stellar group to an ideally symmetric configuration of some effective diameter ρ. In solving (53) additional links like $\sum a_i = \min$ may be applied.

6. Measurements in a specially selected direction

In the previous sections, the behaviour of differential image motion has been studied under conditions of complete averaging of Δ^2 over a couple of angular parameters in the limits $0-2\pi$. When the limits of averaging are not so wide, or the averaging is not performed at all, the properties of differential displacement appear to be essentially different. The reason is the strong anisotropy of the differential displacement $\Delta\xi$, Eq. (8), the power spectrum of which strongly depends on spatial angles ψ, ε, and θ. A main source of anisotropy is averaging phase fluctuations along the wind, which is described by the filter $\mathrm{sinc}^2[\pi VTq\cos(\varphi-\varepsilon)]$.

Let's consider measurements of coordinate differences for a pair of stars at fixed spatial angles, assuming a single-layer model of an atmosphere. Taking into account that integral (17) is a function of $\psi-\varepsilon$ and $\theta-\varepsilon$ differences, the dependence of Δ on $\theta-\varepsilon$ at fixed $\psi-\varepsilon=0$, 15, 45, and 90^0 can be calculated. Figure 3 shows the functions calculated with $\rho=10'$, $T=100$ s, and parameters (22). Graphical data in the region $|\theta-\varepsilon|>10^0$ are well fitted by a function $\Delta_{\max}\sin|\theta-\varepsilon|$, where $\Delta_{\max}$ is the variance at $|\theta-\varepsilon|=90^0$ and some fixed ψ. The horizontal dashed line marks a level of the mean variance Δ_0 in the sense of Eq. (19), with averaging over ψ and θ. Figure 3 shows that at some particular orientations of a baseline (ψ parameter) and ξ-axis (θ angle) the level of Δ can be much lower than Δ_0. There are two cases of interest to be discussed:

1) The baseline AB connecting two stars formes a small angle $|\psi-\varepsilon|<15^0$ with the wind direction, with θ arbitrary;

2) The ξ-axis along which positions are measured is oriented approximately along the wind: $|\theta-\varepsilon|<45^0$, with arbitrary ψ.

Condition (1) essentially limits the number of star pairs which can be measured in the field. For that reason the opportunity (2) that places no limitations on the orientation of baselines is of greater practical value. In the important case of configuration "c", with a central position of a target star, and ψ angle varying over a set of reference stars, this opportunity is unique. Note that improvement in precision expected for ξ-coordinates is achieved at the expense of an equivalent loss in the accuracy of η-coordinates in the perpendicular direction. Such a feature actually causes transition to 1-D mode of measurements. However, it is not necessarily a shortcoming, as for example in parallax programs where only 1-D, high precision differential coordinates are practically of use.

The highest gain in precision for a single-layer atmosphere is expected at $\theta-\varepsilon=0$. In this case evaluation of the integral (17) averaged over ψ in the limits $0-2\pi$ for a small aperture $D\ll h\rho\ll VT$ yields

$$\Delta^2_{\min}=\frac{4\lambda^2 c_\varphi\pi^p(h\rho)^{p+1}}{(1-p^2)(VT)^2}\frac{\Gamma(3/2-p/2)}{\Gamma(3/2+p/2)}. \qquad (55)$$

The ratio $\Delta^2_{\min}/{\Delta_0}^2\approx p(2-p)(1-p^2)^2\rho hV^{-1}T^{-1}$ is proportional to T^{-1} and for long exposures may be rather small. For instance, at $p=2/3$, $h/V=200$ s, $\rho=10'$, and $T=100$ s we have $\Delta^2_{\min}/\Delta^2_0\approx 0.01$. With an exposure increase, the effect is stronger, reflected in Fig. 3 by a sharper minimum at small $\theta-\varepsilon$. It should be noted that effective scales $q_1^{-1}\sim 10^4\rho h\approx 10^5$ m and $q_2^{-1}\sim 10\rho h\approx 10^2$ m of wave-front distortions contributing the best part of Δ^2 are here much longer than in a case of complete double averaging over angular parameters.

For a real multi-layered atmosphere, the transition to measurements in a selected direction is rarely justified, and only under conditions of approximately parallel orientation of wind velocity vectors $\boldsymbol{V}_i$ of all $i=1,2\ldots N$ turbulent layers. In this case, to ensure best filtering of a dominant layer $i=1$ with the greatest index C_n^2, the ξ-axis is positioned parallel to the vector $\boldsymbol{V}_1$ thus ensuring $\theta-\varepsilon=0$. It does not however garantee the decrease of the total variance, which is achieved unconditionally only when $|\varepsilon_i-\varepsilon_1|<45^0$ for each layer i.

An important feature of atmospheric layer distribution in C_n^2 is that at each moment of observations there are only a few layers which greatly dominate over others in the intensity of turbulence (Gendron & Lena 1996; Redfern 1991; Benkhaldoun et al. 1996). This circumstance brings up quasi-single-layer features to the atmospheric behaviour, and is favorable for 1-D techniques of measurements.

Table 3. Examples of vertical turbulence structure, and differential image motion for each layer.

layer No. i	h, km	V, m/s	$\varepsilon_i - \varepsilon$ degr.	$C_n^2\Delta h$, $10^{-14}\mathrm{m}^{1/3}$	Δ_0 mas	Δ mas
1	4	14	0	25.8	11.7	1.31
2	10	59	−8	2.1	2.3	0.47
3	12	51	−9	3.4	3.3	0.78
4	12	44	−13	2.1	2.8	0.91
5	14	33	−4	2.7	3.8	0.62
6	16	36	1	1.9	3.2	0.44
7	17	10	16	1.8	6.1	2.70
8	18	17	37	1.4	4.2	3.51
Caccia et al. (1987)			total:	41	15.5	4.8
1	3	9	−45	15	10.0	10.0
2	6	6	0	28	21.5	4.3
3	10	4	63	9	17.9	21.7
Rocca et al. (1974)			total:	52	29.7	24.3

For discussion we shall consider some observational data. In the upper part of Table 3, Cols. 2–5, are the parameters of atmospheric layers h, V, $|\varepsilon_i - \varepsilon_1|$, and $C_n^2\Delta h$ found by Caccia et al. (1987) from spatiotemporal correlation analysis of single-star scintillations. Observations were obtained with the 1.93 m telescope of the Haute-Provence observatory. In the second part of Table 3, the data found by Rocca et al. (1974) from the analysis of star scintillations on a 10 cm telescope are presented. In Col. 6, Δ_0 values for each layer calculated with Eq. (24) at $T = 100$ s, $p = 2/3$, $\rho = 10'$ and averaged with respect to θ and ψ, are given. Column 7 contains image motion Δ measured in the direction of the vector $\boldsymbol{V}_1$ (that is $\theta = \varepsilon_1$), and also with averaging over ψ. Total values of Δ_0 and Δ integrated over the depth of an atmosphere are also given. The transformation of $C_n^2\Delta h$ into c_ϕ was carried out using Eq. (3) which is valid for 3-D isotropic turbulence.

The vertical structure of an atmosphere which is shown in the first part of the table, at the optimal position of the ξ-axis allows us to reduce the variance of image motion by a factor of 10. In this particular case $|\theta - \varepsilon_i| < 45^0$ for each layer. The wind situation described in the second part of Table 3 is much worse and is characterized by a strong change of the wind orientation with a height. As a result, the contribution of a layer $i = 3$ even encreases, and the total effect $\Delta^2/\Delta_0^2 = 0.65$ for the whole atmosphere becomes negligable.

Barletti gives an even more unfavorable example of the wind shifting 250^0 at heights 13–17 km, where most layers of intense turbulence were concentrated. The vertical profile of the wind velocity given by Hogstrom et al. (1998) for heights 500 m–3 km, on the contrary, has very weak variations of the ε angle, being in the limits $\pm 25^0$.

The above examples show that there is a certain possibility to come across a lucky meteorological situation allowing us to take advantage of anisotropic properties of differential image motion. Detection of atmospheric conditions favourable for a 1-D strategy of observations, however, implies a permanent control of atmospheric parameters using some remote methods of sensing with satisfactory precision of the vertical wind profile determination (Caccia et al. 1987; Rocca et al. 1974).

7. Using r_0 and σ_{30} for calibration of Δ at ill-defined p

When the variance of differential image motion Δ is calculated, calibration is performed with some measured quantity that characterizes the intensity of turbulence. This procedure is however biased because there are usually no reliable data on the p quantity available, so $p = 2/3$ is set tentatively. Besides, we note that there are some quantities that specify the turbulence in a different way, by refering to either one-point or integral estimates of one of the phase-related functions $F_\phi(q)$, $D_\phi(r)$ or $D_n(r)$. Thus, c_ϕ (measured in units of m^{-p-1}) is numerically equal to the function $F_\phi(q)$ at some unit frequency (here 1 m^{-1}) that depends on the adopted system of units; a similar remark concerns C_n^2. More frequently in use are integral estimates such as FWHM, Fried's parameter r_0, and rarely, σ_T.

Let us estimate the bias in Δ caused by assuming $p = 2/3$ when r_0 and σ_{30} are used as normalizing factors. To express r_0 via c_ϕ one may compare the expression for a phase structure function $D_\phi(r) = 2\overline{k}(r/r_0)^{p+1}$ where $\overline{k} = \{8\Gamma[2/(p+1)]/(p+1)\}^{(p+1)/2}$ (Fried 1965) with representation (5). Assuming that the turbulence is completely developed, the use of Eqs. (4–7) yields

$$c_\phi = \frac{(p+1)\overline{k}\Gamma(3/2+p/2)}{2\pi^{2+p}\Gamma(1/2-p/2)} r_0^{-1-p}. \qquad (56)$$

The structure of analytical expressions for Δ^2 derived in the above sections allows us to represent each one (Table 4) as a product of two functions: $K_i(p)$, with a relatively weak dependence on p, and an exponential factor $[S/(VT_{30})]^p$ or $(S/r_0)^p$ which are more sensitive to variations of p. Factors $[D/(VT_{30})]^p$ and $(D/r_0)^p$ appear only for non-symmetric stellar groups like "a" in narrow fields. This representation is valid for both filled apertures and interferometers; in the last case D is to be replaced by d.

With typical $\rho = 1{-}10'$, $h = 2{-}15$ km, $V = 5{-}30$ m/s, $S \sim 1{-}50$ m, and long T we find that $[S/(VT_{30})] < 1$ and $[D/(VT_{30})] < 1$, therefore the derivative $\partial(\Delta^2)/\partial p$ is always negative at any given σ_{30}. On the contrary, when using r_0, expressions for Δ^2 contain ratios $S/r_0 > 1$ and $D/r_0 > 1$, so in this case $\partial(\Delta^2)/\partial p > 0$. Considering that usually $1/3 < p < 2/3$ (Sect. 3), we find $\Delta(p) > \Delta(2/3)$, where $\Delta(p)$ is the actual value of Δ, and $\Delta(2/3)$ is that calculated with $p = 2/3$ and measured σ_{30}. Using r_0 results in inverse inequality $\Delta(p) > \Delta(2/3)$.

Figure 4 presents numerical estimates made for two atmospheric layers with $h = 2.8$ km, $V = 14$ m/s (solid) and $h = 15$ km, $V = 30$ m/s (dashed), double star "a" at wide separation $\rho = 10'$, $T = 100$ s, and $D \ll S$. The functions $\Delta(p)$ calculated with fixed $\sigma_{30} = 0.14''$ (both layers) show strong dependence on p, so the actual variance

Table 4. The structure of expressions for Δ^2 as functions of p with normalizing parameters c_ϕ, $C_n^2\Delta h$, σ_{30} and r_0, and derivates $\partial(\Delta^2)/\partial p$.

Parameter	$S \gg D$, all conf.-s; $S \ll D$, symm. conf.-s	$S \ll D$, conf. "a"	$\partial(\Delta^2)/\partial p$
c_ϕ	$\lambda^2 c_\phi K_1(p) S^p$	$\lambda^2 c_\phi K_5(p) D^p$	-
$C_n^2\Delta h$	$C_n^2\Delta h K_2(p) S^p$	$C_n^2\Delta h K_6(p) D^p$	-
σ_{30}	$\sigma_{30}^2 K_3(p)[S/(VT_{30})]^p$	$\sigma_{30} K_7(p)[D/(VT_{30})]^p$	< 0
r_0	$\lambda^2 r_0^{-1} K_4(p)(S/r_0)^p$	$\lambda^2 r_0^{-1} K_8(p)(D/r_0)^p$	> 0

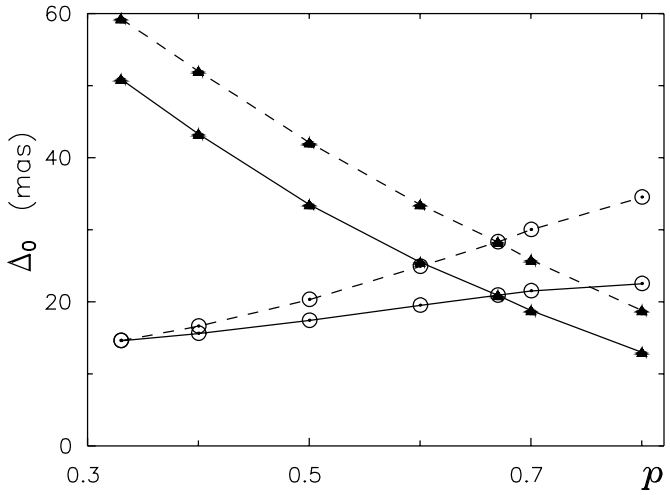

Fig. 4. The variance Δ_0 as a function of p for binary star "a", $\rho = 10'$, $T = 100$ s, $h\rho \gg D$. Calibration based on $r_0 = \text{const}$ (circles) or $\sigma_{30} = \text{const}$ (triangles). Solid lines: atmospheric layer $h = 2.8$ km, $V = 14$ m/s, $r_0 = 83$ mm (or $\sigma_{30} = 0.14''$); dashed: $h = 15$ km, $V = 30$ m/s, $r_0 = 71$ mm (or $\sigma_{30} = 0.14''$).

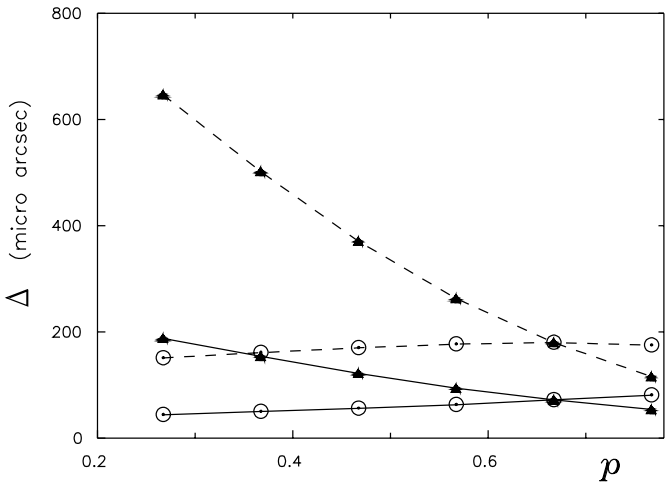

Fig. 5. The same as in Fig. 4, for interferometer with a baseline $d = 10$ m (dashed) and filled aperture $D = 10$ m (solid), for triple star "b", $\rho = 1'$, $T = 100$ s; lower atmopheric layer is considered.

$\Delta(p)$ may exceed 100% of its prediction $\Delta(2/3)$. Plotting curves with fixed r_0, we used quantities $r_0 = 83$ mm (lower layer) and $r_0 = 71$ mm (higher layer), both correponding to $\sigma_{30} = 0.14''$ at the point $p = 2/3$. These data are more stable concerning p variations, the bias not exceeding 50%. Better results are due here to adjacent positions of the spectral subranges which account for Δ and r_0 quantities generation, effective frequencies for σ_{30} being much lower. Figure 5 shows the functions $\Delta(p)$ for interferometer $d = 10$ m (dashed) and filled aperture $D = 10$ m (solid) calculated with $\rho = 1'$ and $T = 100$ s for the triple star "b" (lower atmospheric layer). The behaviour of these functions representing the accuracy of symmetric stellar group observations in very narrow fields is similar to that seen in Fig. 4 (large S and asymmetric configuration "a"), which reflects the similarity in the structure of relevant expressions for Δ in Table 4.

In Table 5 we reproduce data of Table 2 for the non-Kolmogorov spectral index $p = 1/3$ and the former value of $r_0 = 83$ mm. Comparison of Tables 2 and 5 shows that the largest change of image motion magnitude occures when double-star separations are measured. Owing to the dependence $\Delta^2 \sim (D/r_0)^p$, the effect is stronger for large $D \sim 100{-}1000 r_0$ telescopes. Concerning symmetric stellar groups, one may note comparatively stable estimates of Δ, especially for interferometers.

8. Conclusions

In this Paper we derive necessary formulations and analyze some effects which may be useful for understanding the properties of differential image motion under non-Kolmogorov distortions of the wave-front. Non-classic statistics of the turbulent phase are due to three effects: non-Kolmogorov type of refractive index n fluctuations in 3-D space, 2-D spatial location of a turbulence, and wind-dependent anisotropy of the phase. The two first sources result in the decrease of p; the effect becomes stronger at large scales. According to observational data, on scales 1–300 m which are effective for differential image motion, p is typically in the range 1/3–2/3. Deviation of p from its Kolmogorov value 2/3 affects all phase-related quantities, in particular, causes divergence of the observed Δ value from that calculated at $p = 2/3$. The bias may exceed 50% or more, depending on which quantity, r_0 or σ_{30}, is taken as a measure of the intensity of turbulence (Figs. 4 and 5), and which stellar configuration is observed. Thus, when measuring double-star separations, Δ^2 is proportional to the factors $(D/r_0)^p$ and $(d/r_0)^p$ which practically do not depend on p for small instruments. The situation is quite different for the Keck 10 m telescope and some operating

interferometers with $d \sim 100$ m, when small 1/3 to 2/3 variations of p evoke a change of 5–10 in Δ^2, better accuracies corresponding to small p.

Table 5. The same as in Table 2, at $p = 1/3$ and $r_0 = 83$ mm.

conf.-n	offset	interferometer, d		filled pupil, D	
type	ρ'	10 m	100 m	10 m	100 m
"a"	-	1230	180	850	120
"b"	0	160	16	48	1.5
"c"	0	150	15	25	0.8
"b"	$15''$	350	48	220	30

In brief, we analyzed a third factor of non-Kolmogorov distortions of the wave-front, a spatial anisotropy of the phase brought in by the wind. We concluded that at certain conditions it may be useful for improving the accuracy of ground-based observations. Examples given in the upper part of Table 3 show that the use of a special 1-D strategy of measurements which takes advantage of anisotropic properties of the turbulent phase may result in a perceptible reduction of Δ.

Rather unexpected results have been obtained when studying the peformance of a classic circular pupil. Expressions derived for Δ do not follow power laws predicted by Lindegren (1980) as his analysis is directly valid for interferometers. For symmetric stellar groups ("b" or "c") measured in very narrow fields, a new power law derived $\Delta^2 \sim S^{3+p}D^{-3}$ differs by a factor of S/D from Lindegren's dependence $\Delta^2 \sim S^{2+p}D^{-2}$. This circumstance results in an order smaller, as compared to current, estimates of Δ for observations with very large $D \sim 10{-}100$ m apertures and small $\sim 1'$ angles (Tables 2 and 5).

High-accuracy differential astrometry is required primarily to study double-stars, determination of parallaxes, and in searching for extrasolar planets. These problems can be solved very effectively with future astrometric satellites that will have an expected accuracy of about 1–10 μas. The potential of ground-based astronomy also looks rather promising, considering projects of large-scale facilities. The analysis of atmospheric effects made in this Paper allows us to conclude that this source of errors can be reduced approximately to the level expected for space missions, or 1 μas per 100 s exposure.

The largest operating 10 m Keck telescope has a potential narrow-field accuracy of 30–70 μas per 100 s exposure at the Kolmogorov parameter p (Table 2), and 20–50 μas at $p = 1/3$ (Table 5). Due to a strong $\Delta \sim D^{-3/2}$ improvemnt with D, the 1 μas per 100 s time level is already expected at $D = 100$ m. For interferometers, baselines of about 1000 m are required because of the slower improvement of $\Delta \sim d^{-1}$. Interferometers of this class should be able to measure simultaneously at least three objects so as to detect a minimal symmetric configuration of stars. Interferometers of the Mark III type with two separate beam channels are restricted to observations of asymmetric double-star systems, and even at $d = 1000$ m baselines will be limited by $\Delta \sim 20{-}40$ μas (Sect. 5.3).

The above estimates relate to the dimeter $\rho = 1'$ of the reference group; in other cases correction allowing for dependences $\Delta \sim \rho^{(3+p)/2}$ (filled apertures) and $\Delta \sim \rho^{(2+p)/2}$ (interferometers) should be applied. Very high accuracies, however, require perfect centering of the reference frame on the target object. Even very small $\rho = 1''$ offsets will generate, depending on p, errors of 2–5 μas for a $D = 10$ m telescope (Sect. 5.3), and about 0.5–1 μas with $D = 100$ m. Errors of this type are completely eliminated with the symmetrizing procedure (Sect. 5.4). An extra 1.5–2 fold improvement is expected at astronomical sites with average $p \leq 1/3$ on spatial scales 1–300 m.

References

Armstrong, J. W., & Sramek, R. A. 1982, Radio Sci., 17, 1579
Barletti, R., Ceppatelli, G., Paterno, L., et al. 1977, A&A, 54, 649
Benkhaldoun, Z., Jabiry, A., & Vermin, J. 1996, ApSS, 239, 237
Bester, M., Danchi, W. C., Degiacomi, C. G., et al. 1992, ApJ, 392, 357
Bull, G. 1967, in ed. A. M. Yaglom, & V. I. Tatarsky, Atmospheric turbulence and radio wave propagation. Proceedings of the inernational colloquium (Nauka, Moscow), 206
Buscher, D. F., Armstrong, J. T., Hummel, C. A., et al. 1995, Appl. Opt., 34, 1081
Caccia, J. L., Azouit, M., & Vernin, J. 1987, Appl. Opt., 26, 1288
Chunchuzov, I. P. 1996, J. Atmos. Sci., 53, 1798
Conan, J., Rousset, G., & Madec, P. 1995, JOSA A, 12, 1559
Coulman, C. E., Vernin, J., Coqueugniot, Y., & Caccia, J. L. 1988, Appl. Opt., 27, 155
Coulman, C. E., & Vernin, J. 1991, Appl. Opt., 30, 118
Dalaudier, F., & Sidi, C. 1987, J. Atmos. Sci., 44, 3121
Fried, D. L. 1965, JOSA, 55, 1427
Gatewood, G. D. 1987, AJ, 94, 213
Gendron, E., & Lena, P. 1996, ApSS, 239, 221
Goodman, J. W. 1985, Statistical optics (Wiley-Interscience publication, New York)
Han, I. 1989, AJ, 97, 607
Hog, E. 1968, Z. Astrophys., 69, 313
Hogstrom, U., Smedman, A., & Bergstrom, H. 1998, J. Atmos. Sci., 56, 959
Lazorenko, P. F. 1992, Kin. Phys. Celest. Bodies, 3, 78
Lilly, D. K. 1983, J. Atmos. Sci., 40, 749
Lindegren, L. 1980, A&A, 89, 41
Lumley, J. L., & Panofsky, H. A. 1964, The structure of atmospheric turbulence (Interscience publishers, New York)
Martin, H. M. 1987, PASP, 99, 1360
Redfern, R. M. 1991, Vistas Astron., 34, 201
Rocca, A., Roddier, F., & Vernin, J. 1974, JOSA, 64, 1000
Sarazin, M., & Roddier, F. 1990, A&A, 227, 294
Shao, M., & Colavita, M. M. 1992, A&A, 262, 353
Tatarsky, V. I. 1961, Wave propagation in a turbulent medium (Dover, New York)
Vinnichenko, N. K., Pinus, N. Z., Shmeter, S. M., & Shur, G. N. 1976, The turbulence in a free atmosphere (Hydrometeoizdat, Leningrad)
Weinstock, J. 1980, J. Atmos. Sci., 37, 1542